Water Science & Technology

IWA PUBLISHING



Water Science & Technology Vol 84 No 3, 763 doi: 10.2166/wst.2021.265

# Photocatalytic degradation of hydroxychloroquine using ZnO supported on clinoptilolite zeolite

Patricia Lacchi da Silva[a], Ramiro Picoli Nippes[a,*], Paula Derksen Macruz[a], Fábio Luís Hegeto[b] and Mara Heloísa Neves Olsen Scaliante[a]

[a] Department of Chemical Engineering, State University of Maringa, Maringa 87020-900, Parana, Brazil
[b] Physics Department, State University of Maringa, Maringa 87020-900, Parana, Brazil
*Corresponding author. E-mail: ramiro_picoli@yahoo.com.br

RPN, 0000-0002-9919-003X; PDM, 0000-0002-5474-7017; MHNOS, 0000-0001-9090-9274

## ABSTRACT

The objective of this work was to evaluate the photocatalytic activity of zinc oxide catalysts supported on natural zeolite clinoptilolite for photocatalytic degradation of the drug hydroxychloroquine, used in the treatment of malaria and which has been tested in the treatment of COVID-19. To synthesize 10%ZnOCP and 15%ZnOCP catalysts, the wet impregnation methodology was used. The raw and synthesized catalysts were characterized by XRD, SEM, XRF, BET, DRS, PCZ, FT-IR and PL. The degradation of hydroxychloroquine was calculated using UV-vis absorption from the samples before and after the photocatalytic process. The maximum percentage of degradation (96%) was obtained with the operational parameters of $C_0 = 10$ mg $L^{-1}$; $C_{cat} = 2$ g $L^{-1}$ of 15%ZnOCP; pH = 7.5; UV-A radiation. Ecotoxicological tests against the bioindicators *Lactuca sativa* and *Artemia salina* confirmed the reduction of effluent toxicity after treatment.

**Key words:** catalysis, clinoptilolite, hydroxychloroquine, waste water

## HIGHLIGHTS

- A ZnO-based photocatalyst supported on natural zeolite was synthesized for degradation of hydroxychloroquine (HCQ).
- High degradation efficiency (96%) of HCQ using the 15%ZnOCP catalyst.
- Reduction of effluent toxicity after photocatalysis treatment.
- 15%ZnOCP did not significantly reduce its photoactivity after first use.
- The 15%ZnOCP catalyst was also efficient under natural solar radiation.

## GRAPHICAL ABSTRACT

## 1. INTRODUCTION

Water pollution is one of the biggest challenges facing humanity, especially when it comes to the retention of persistent pollutants in aquatic matrices, such as herbicides, hormones and drugs. Among medications, hydroxychloroquine is an important chiral drug used mainly in the treatment of rheumatoid arthritis, lupus and malaria, and has been studied for its use in combating the disease caused by the new coronavirus (Borba *et al.* 2020). The possibility of using the drug in the treatment of COVID-19 has led to an increase in its consumption worldwide enhanced by the not recommended practice of self-medication (Chen *et al.* 2020).

Like other drugs, hydroxychloroquine is not fully metabolized by the body, being excreted in the urine (25–30%) in its inactive form or metabolites (Browning 2014), reaching sewage systems and consequently effluent treatment plants, which have limitations in the elimination of this compound. The potential for environmental persistence of hydroxychloroquine has been reported in the literature, since it is a compound with high solubility and low degradation (Daughton 2014).

Therefore, it is of fundamental importance to study processes that can effectively remove hydroxychloroquine from water, such as heterogeneous photocatalysis, which stands out for its efficiency in degrading a range of pollutants with low biodegradation, the possibility of reusing the catalyst and low cost. However, there have been few studies that address the photocatalytic degradation of hydroxychloroquine. Thus, the objective of this study was to fill this gap and overcome some problems associated with the heterogeneous photocatalysis process, such as the recombination of the electron-hole pair and the difficulty in recovering the catalyst after the process, because the main semiconductors used ($TiO_2$ and ZnO) are very thin powders (Sacco *et al.* 2018). Among the most used semiconductors, ZnO stands out as a photocatalyst due to its unique properties such as stability, high optical sensitivity, low-cost characteristics and non-toxic nature (Heidari *et al.* 2020).

To overcome the difficulty in ZnO recovery, the technique of synthesizing supported catalysts has stood out, as supported photocatalysts with high adsorption capacity have excellent advantages, including a decrease in the recombination rate of photogenerated electron-hole pairs and photocatalyst recovery due the increase in particle size (Bahrami & Nezamzadeh-Ejhieh 2015). Among the supports used, zeolites have stood out because they present appreciable characteristics such as acidity, high surface area and thermal stability, and even antibacterial activity (Nezamzadeh-Ejhieh & Khodabakhshi-Chermahini 2014). In this context, the use of natural clinoptilolite zeolite has shown promise as a catalyst support due to its low cost, abundant pores and channels, as well as excellent adsorption capacity, in addition to being one of the most widely distributed zeolites on the planet (Shen *et al.* 2020).

Given the above, this work aimed to synthesize and characterize a material based on the heterojunction of ZnO and clinoptilolite natural zeolite in order to unite the adsorption potential of natural zeolite with the photocatalytic potential of ZnO for the efficient removal of the drug hydroxychloroquine and evaluate the reduction of its toxicity after treatment.

## 2. MATERIALS AND METHODS

### 2.1. Materials and used chemicals

Zeólita natural Clinoptilolita (CP) was provided by the company Celta Brasil located in Vila Jovina – Cotia/SP, 06705150. CP is mainly composed of $SiO_2$ and $Al_2O_3$. Before the experimental tests, the zeolite was washed with deionized water, dried in an oven and sieved (0.4–1.0 mm). Zinc oxide (99%) was obtained from Synth and hydroxychloroquine (HCQ) (>98%) was obtained from Sigma-Aldrich. Reverse osmosis water was used to prepare the solutions.

### 2.2. Preparation of supported catalysts

The process of synthesis of the catalyst supported by CP was similar to the methodology of Zhao & Yu (2006) of wet impregnation. The CP was washed and dried in an oven at 80 °C for 12 h. Zinc oxide was solubilized in distilled water in the desired mass percentage (10 and 15%) and then was added to the zeolite. The mixture was stirred at room temperature for 16 h on the rotary vacuum evaporator at a temperature of 80 °C, until the material was completely dried. Then, the catalyst was placed in an oven for 24 h at 80 °C. The catalyst was calcined in the muffle at 500 °C for 5 hours. Finally, the catalyst was passed through a 35-mesh sieve to separate the catalyst that was fragmented during rotary evaporation, standardizing the granulometry (0.50 mm).

### 2.3. Characterization of catalysts

The catalysts were characterized by X-ray diffraction (XRD) analysis on a Shimadzu XRD 6000 device, using copper as the irradiation source (K$\alpha$ 15,406 Å). The scanning speed was 2° per minute with a step of 0.02°, a voltage of 40 kV and an electric current of 30 mA in the range of 5–85° (2$\theta$).

Scanning electron microscopy (SEM) analyzes were performed on a FEI Company, model Quanta-250 scanning electron microscope using 20 kV beam acceleration. The samples were metallized with gold using the metallic coating equipment Sputter Coater Emitech, model K450.

X-ray fluorescence spectroscopy (XRF) analyzes were performed in the Rigaku ZSX Primus II equipment, using oxide standards. To perform the measurements, the samples were pelleted using boric acid as support.

Specific area and pore volume were determined on a Quanta Chrome NOVA 1,200 specific area meter by nitrogen (Linde >99.999% purity) physisorption analysis at 77 K and pressures from $1.2 \times 10^{-3}$ up to 0.092 MPa using the analyzer Micromeritics ASAP 2020. Prior to the analysis, the sample was degassed at $1.3 \times 10^{-4}$ MPa and 300 °C, for 6 h. The specific area was determined using the BET equation and the pore volume was calculated using single point adsorption at $P/P_0 = 1$. The pore volume was obtained from the BJH desorption cumulative volume of pores. The average pore diameter was estimated using the desorption branch of the isotherm and the BJH model.

The analysis of diffuse reflectance spectroscopy in the UV-Visible (DRS) region was performed on an Evolution Array Thermo Scientific spectrophotometer using $BaSO_4$ powder as a reference material at wavelengths of 200–1,100 nm. The samples were solubilized in water and dispersed in a vortex mixer. The band-gap values of photocatalysts were determined through the corresponding Kubelka–Munk function (KM) (which is proportional to the absorption of radiation) and by plotting $(KM \times h\upsilon)^2$ against $h\upsilon$.

To determine the zero-charge point ($pH_{ZCP}$) a Bell bench pH meter and a Marconi shaker table were used. The methodology was based on the '11-point experiment' method. Eleven Erlenmeyer flasks were used with 50 mL of deionized water adjusted to 11 different pH values (2, 3, 4, 5, 6, 7, 8, 9, 10, 11, 12) with solutions of hydrochloric acid or sodium hydroxide 0.1 mol $L^{-1}$. In each Erlenmeyer flask, 50 mg of catalyst were added and taken to shake in a Shaker-type incubator (Marconi) at 120 rpm and 25 °C for 24 hours. Finally, the final pH was measured for each Erlenmeyer flask and a graph of the final pH was plotted against the initial pH, by which it was possible to determine the $pH_{ZCP}$ value.

The spectroscopy analysis in the infrared region (FT-IR) was performed on a Bruker–Vertex 70 spectrophotometer in the 4,000–400 $cm^{-1}$ range. KBr was used as a reference, 100% transmittance and, for analysis, 0.002 g of sample were weighed and mixed in 0.198 g of KBr.

The photoluminescence spectroscopy (PL) technique was performed on a Perkin Elmer luminescence spectrometer, LS-50B. The samples were excited at a wavelength of 320 nm and the reading was performed in a spectral region of 350–600 nm.

### 2.4. Experimental tests

The photocatalytic tests were carried out in two different reaction units shown in Figure S1 (Supplementary information). The artificial light reactor consists of a steel box to isolate radiation to the environment, covered with aluminum paper and equipped with two side fans for internal cooling. The radiation source consists of five UV-A (black light) tubular fluorescent lamps, measuring 26 mm × 450 mm, with a power of 45 W and luminous intensity of 0.061 W $m^{-2}$ positioned at the top of the box at a distance of 15 cm. The bottom of the box was made up of a magnetic stirrer and the aliquots were removed through hoses on the side of the box. The natural sunlight reactor consisted of a reaction system disposed in the external environment, with no interference such as trees and buildings, so that it received solar radiation directly. The tests were carried out on the campus of the State University of Maringá in the city of Maringá-PR (23°25′31′S, 51°56′19′W). The average values of temperature and radiation during the experiments provided by the Main Climatological Station of Maringá (ECPM) corresponded to 27.8 °C and 2,493.92 kJ/m², respectively. A pyrex glass reactor, with a capacity of 500 mL, was equipped with a magnetic stirrer and surrounded by an aluminum cone to direct the received radiation. The reactions were carried out between 11 and 14 hours, at room pressure and temperature.

The reaction volume used corresponded to 250 mL. Catalysts synthesized at concentrations of 1–3 g $L^{-1}$ were used. The reaction time consisted of 30 minutes of adsorption in the dark and then 3 hours of photocatalytic reaction with the light on. The 2.5 mL aliquots were collected every 30 minutes and filtered using 0.22 μm membranes (Millipore) to monitor photodegradation. All experiments were carried out in triplicate.

The residual HCQ concentration was analyzed on a UV-Vis spectrophotometer (Shimadzu – model UV-1800), at $\lambda =$ 220 nm. The concentration of the contaminant was calculated by reading the absorbance at the wavelength, and it was determined using the equation corresponding to the calibration curve. The percentage of degradation was calculated using Equation (1), where $C_0$ is the initial concentration of the sample and $C_t$ is the concentration at time t:

$$D(\%) = \left(\frac{C_t - C_0}{C_t}\right) \times 100 \quad (1)$$

### 2.5. Toxicity tests

The best degradation condition of HCQ was submitted to toxicological tests against the bioindicators *Artemia salina* and *Lactuca sativa*. Both indicators showed a rapid response under a small amount of contaminant.

To germinate the seeds of *Lactuca sativa*, the USEPA (1996) guideline was followed. Ten seeds were placed under filter paper prepared in Petri dishes. Three milliliters of treated effluent, without dilution, were added to the plate. A negative control was performed with distilled water and a positive control with three different concentrations of sodium chloride (2 M, 1 M, 0.5 M). The plates were left in the dark for 120 hours at 25 °C. The tests were considered valid when the germination of the seeds of the negative control was equal to or greater than 65% and the roots reached at least 5 mm. After 120 hours of exposure, the number of germinated seeds was counted and the length of the roots measured with the aid of a scale. The relative germination rate (RGR) was calculated using Equation (2), taking into account the ratio of the number of germinated seeds to the total number of seeds and the relative length rate (RLR) was calculated using Equation (3), considering the ratio of the average root length of the samples to the average root length of the control plate:

$$RGR = \frac{n^{o}\ of\ germinated\ seeds}{n^{o}\ total\ seeds} \times 100 \quad (2)$$

$$RLR = \frac{average\ root\ length}{mean\ root\ length\ in\ the\ control} \times 100 \quad (3)$$

The guideline for hatching *Artemia salina* cysts followed the precursor methodology of Meyer *et al.* (1982) in which the cysts were incubated in saline solution prepared with sea salt at a concentration of 35 g $L^{-1}$ for 48 h at 28 °C with continuous lighting and aeration. After hatching, the most active organisms were separated from cysts that did not hatch using a light beam directed at these organisms for over 24 h. For toxicity tests, ten larvae of *Artemia salina* were transferred with the aid of a dropper, to a multi-well plates containing 35 g $L^{-1}$ of saline solution and 1 g $L^{-1}$ of potassium dichromate at five different concentrations (0, 10, 20, 40 and 60 mL), which corresponded to the control plate (toxic reference) and ten more larvae were added to another multi-well plate containing 35 g $L^{-1}$ saline solutions prepared with a sample to be tested at six different concentrations (0, 0.1, 0.3, 0.7, 1 and 2 mL), which corresponds to the sample plate. The plates were kept for 24 hours in the dark and the tests were performed in triplicate. Mortality of nauplii was assessed and, when the rate was greater than 50%, it was possible to determine the $LC_{50}$ from the Reed–Muench graph. The test was considered valid if the mortality in the control did not exceed 10%.

## 3. RESULTS AND DISCUSSION

### 3.1. Characterization of catalysts

The XRD patterns of the synthesized catalysts, the CP and the pure ZnO are provided in Figure 1. The XRD spectrum of the CP reveals the diffraction peaks with monocyclic crystal phase ($2\theta = 9.8$, 11.1, 22, 3, 22.7, 26.0, 28.1, 30.0 and 32.0°) in accordance with the JCPDS sheet no. 00-025-1349. For ZnO, the diffraction peaks corresponding to the JCPDS sheet no. 03-065-3411 ($2\theta = 31.8$, 34.3, 36.3, 47.3, 57.8, 62.5, 66.3, 67.6, 69.0, 72.2 and 77.0°) confirm the formation of zinc with the hexagonal structure of the wurtzite belonging to the space group P63mc. It is possible to observe that the peaks present in the XRD of zinc oxide supported in zeolite decrease when compared to the peaks present in the zinc oxide powder, an effect which is related to the low loading of ZnO in the zeolite structure and their overlapping with the diffraction peaks of the zeolite in this region (Heidari *et al.* 2020).

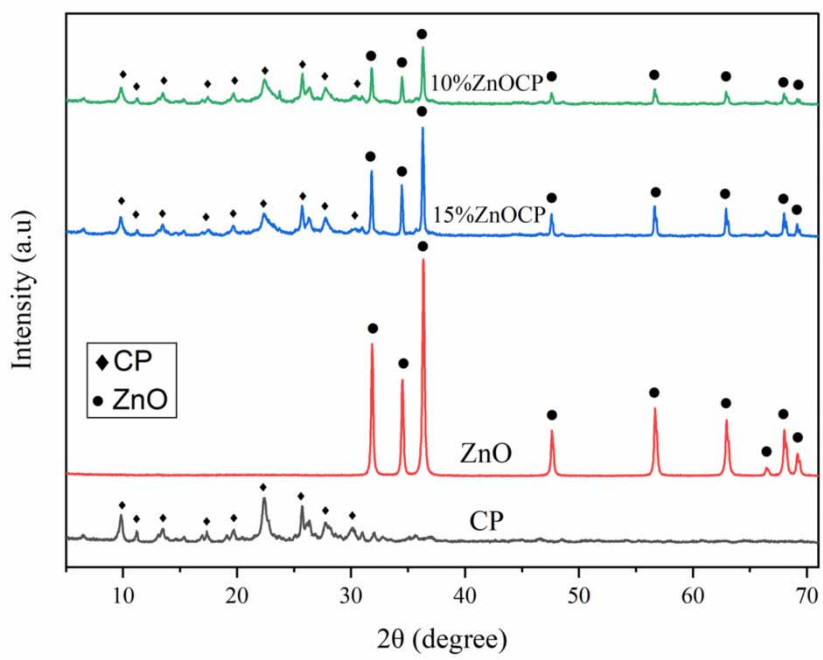


**Figure 1** | XRD patterns of the particles and synthetized catalysts.

The morphology of CP, 10%ZnOCP and 15%ZnOCP catalysts can be seen in Figure 2(a)–2(c), respectively, through micrographs with a magnification of ×10,000. For the CP it was possible to observe a relatively smooth irregular surface with a leaf structure (Shen *et al.* 2020), some light spots of small size corresponded to cavities and voids in the natural clinoptilolite. For samples incorporated with ZnO, it is possible to observe a dispersion of ZnO particles, which cover the clinoptilolite surface and its surface becomes rough. With the increase in the amount of ZnO, a greater agglomeration of particles was observed and a greater perception that the pores of the zeolite were blocked by ZnO and the porosity of the catalyst decreased. The coating of zeolite particles by ZnO confirmed its participation in the photocatalysis phenomena (Nezamzadeh-Ejhieh & Khodabakhshi-Chermahini 2014). The surface compositions of the supported catalysts were determined by XRF analysis (Table S1 – Supporting Information) which shows that the ZnO content on the CP surface was close to the desired theoretical value for the 10%ZnOCP and 15%ZnOCP catalysts. SEM images showed that the coverage of ZnO particles in 15%ZnOCP was greater than that of 10%ZnOCP, being consistent with the XRF analysis.

The textural properties of the CP, ZnO, 10%ZnOCP and 15%ZnOCP were determined by the physisorption of $N_2$ and the results obtained are summarized in Table 1. A reduction in the specific area and pore volume is observed for the catalysts supported in CP, due to the effect of the incorporation of ZnO, which blocks some pores of the zeolite (Nezamzadeh-Ejhieh & Khodabakhshi-Chermahini 2014). The increase in the average pore diameter of the supported catalysts, in theory, is advantageous, since it improves the adsorption capacity, contributing to the formation of a synergistic system of adsorption–degradation (Tan *et al.* 2020). The UV-vis DRS analysis was used to determine the value referring to band-gap energy and thus evaluate the effects of incorporation of zinc oxide particles in the CP zeolite structure. The incorporation of ZnO in the zeolite CP resulted in a small increase in the energy of the band gap, as shown in Table 1. This change in the energy of the band gap in catalysts supported on zeolites may be related to the size of the crystal and the ZnO load employed. The incorporation of ZnO in the zeolite can affect the crystallite sizes of ZnO, making them smaller and increasing the energy of the band gap, this can be linked to the quantum confinement effect (Piedra López *et al.* 2021). The $pH_{ZCP}$ are also show in Table 1 and means that for pH values below and above the $pH_{ZCP}$ obtained, the catalyst surface has positive and negative charges, respectively (Batistela *et al.* 2017). For catalysts supported on zeolite, a reduction in the $pH_{ZCP}$ value was noticeable, which confirmed that the support alters the $pH_{ZCP}$ for ZnO, as reported in other studies (Bahrami & Nezamzadeh-Ejhieh 2015; Heidari *et al.* 2020). The zero-charge point (ZCP) of the supported catalysts was around 6.2, which indicated that the surface will be negatively charged in any pH above this value. The solution with the HCQ molecule has

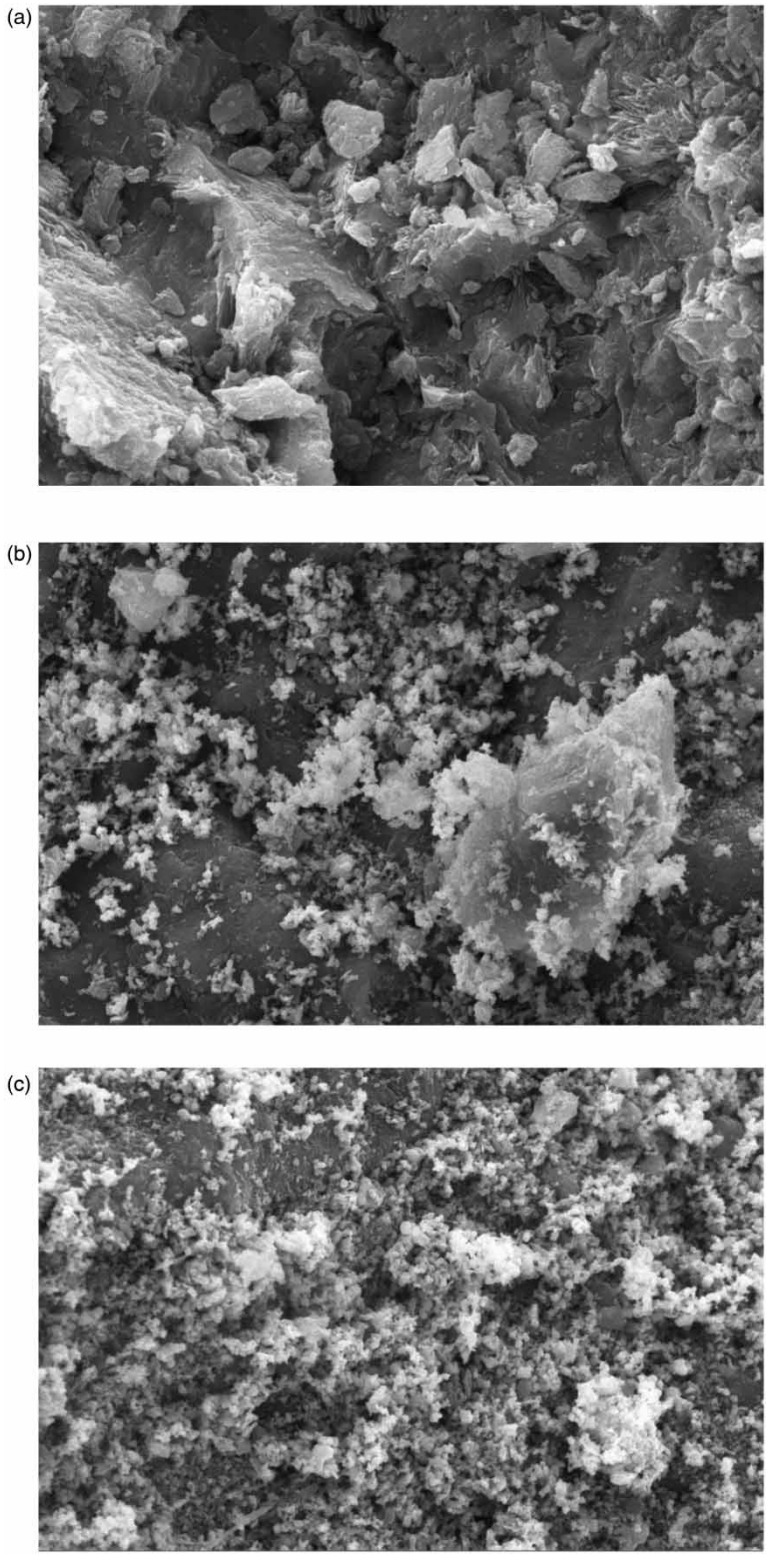


**Figure 2** | Micrograph of (a) CP, (b) 10%ZnOCP and (c) 15%ZnOCP.

a natural pH of 7.5 and its pKa is estimated as 9.67, so its molecules will be positively charged. This difference in loads favors the adsorption of HCQ on the surface of the catalysts, where hydroxyl radicals are generated, which could favor the degradation process.

**Table 1** | Textural parameters, band-gap energy and $pH_{ZCP}$ for all samples

| Sample | $S_{BET}$ ($m^2/g$)[a] | V ($cm^3/g$)[b] | d (nm)[c] | Band gap (eV)[d] | $pH^e_{ZCP}$ |
|---|---|---|---|---|---|
| CP | 131.17 | 0.083 | 2.5 | – | 7.2 |
| ZnO | 3 | 0.014 | 10.8 | 3.13 | 8.43 |
| 10%ZnOCP | 44.03 | 0.043 | 4.9 | 3.20 | 6.2 |
| 15%ZnOCP | 35.22 | 0.059 | 5.3 | 3.22 | 6.3 |

a, BET specific area; b, pore volume; c, pore diameter; d, band gap energy; e, zero-charge point.

Figure 3 shows the infrared spectrum of the materials. It is possible to verify the presence of a band in the region of 3,434–3,643 $cm^{-1}$ in all spectra. For the CP sample, this band corresponds to the OH groups bridged in Al–OH–Si and is attributed to the location of the hydrogen atoms in different oxygen atoms in the structure, while for ZnO the presence of hydroxyl groups is attributed (O–H). The peak located at 1,641 $cm^{-1}$ in the CP spectrum is attributed to the tensile vibrations of the carbonyl functional group (C = O), while for ZnO it is attributed to hydrogen bonding (Gutul *et al.* 2014). For ZnO, the characteristic absorption peak at 540 $cm^{-1}$ is attributed to Zn-O corresponding to the metal-oxygen vibration mode. The peaks at 875 and 1,027 $cm^{-1}$ can be attributed to the elongation modes –C–O and –C–O–C– (Dobrucka & Długaszewska 2016). For clinoptilolite, characteristic absorption bands of the material are found, such as the asymmetrical elongation of the external tetrahedral bond (1,043 $cm^{-1}$), the symmetrical tetrahedral elongation (460 $cm^{-1}$) and connections between the $SiO_4$ tetrahedrons (788 and 609 $cm^{-1}$) (Trujillo *et al.* 2013). The permanence of the characteristic clinoptilolite absorption bands after incorporation of the ZnO semiconductor strongly suggests a stability of the natural zeolite structure during the incorporation process.

Photoluminescence spectroscopy (PL) was used to analyze the presence of defects and the rate of recombination of ZnO and ZnO supported by CP zeolite. The technique was also used for pure CP. Figure 4(a) shows the result of photoluminescence for ZnO catalysts and Figure 4(b) for pure CP. For pure ZnO there is a first strong and narrow peak in the UV region, at approximately 387 nm, referring to the peak of ZnO emission near the edge of the band, as the energy corresponding to this peak is almost equal to the energy of the gap for ZnO (Roychowdhury *et al.* 2013), and two other less intense peaks located at 479 and 524 nm. The blue emission band in the visible at 479 nm was attributed to the electronic transition from the Zni level

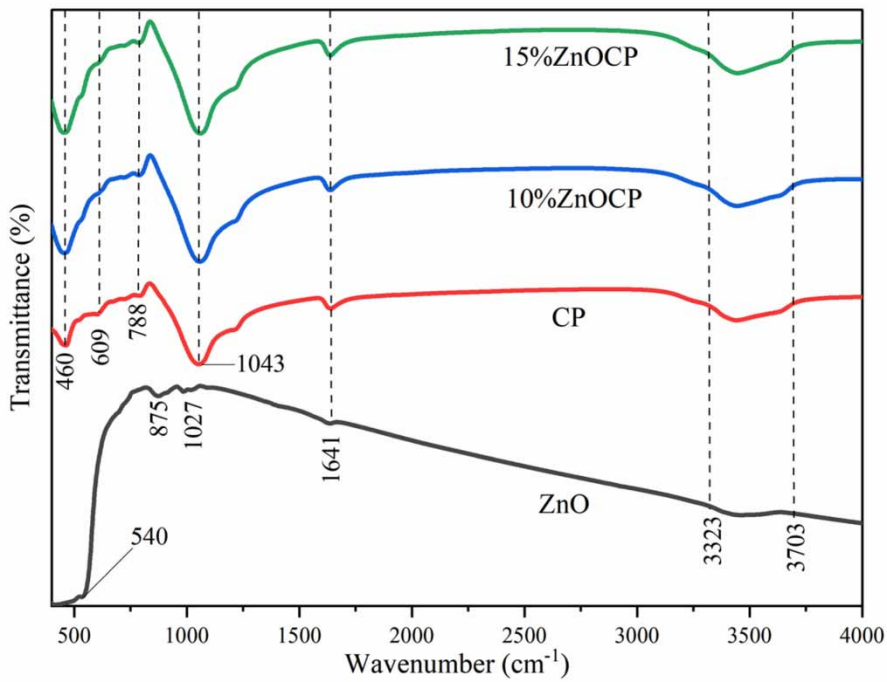


**Figure 3** | Infrared spectra for ZnO, clinoptilolite and the catalysts supported in zeolite.

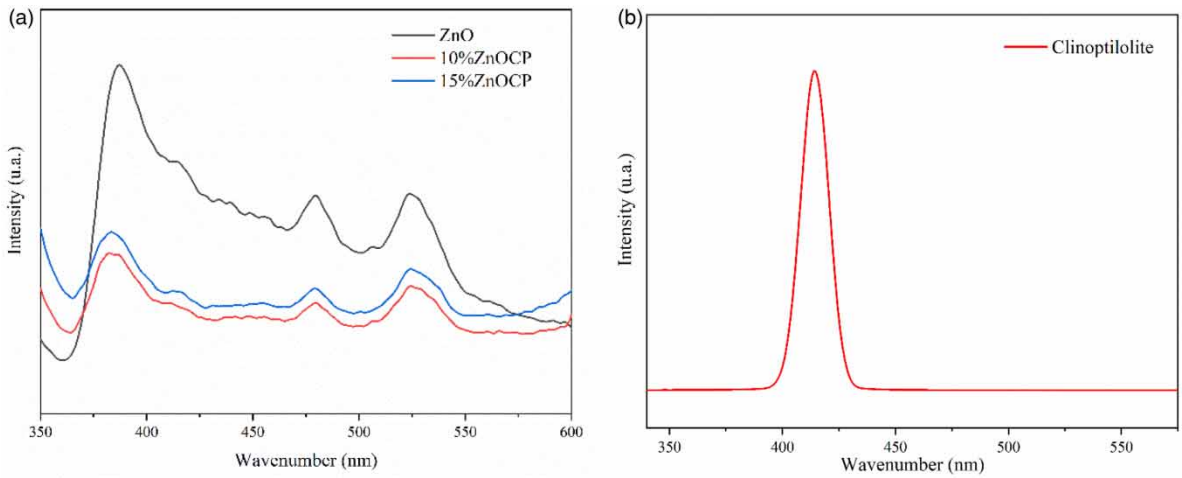


**Figure 4** | Photoluminescence spectra of catalysts (a) ZnO, 10%ZnOCP, 15%ZnOCP and (b) CP.

to the VZn level (Rathore *et al.* 2017). The green emission band at 524 nm, according to the literature, is attributed to an electronic transition from the lower part of the conduction band to the VO level (Roychowdhury *et al.* 2013). Assessing the spectra of pure ZnO and ZnO supported on CP, it is clear that, for pure ZnO, the spectra presented greater intensity than the supported catalysts, which leads to the hypothesis that this sample provides a greater unfavorable recombination of $e^-/h^+$. The reduction in peak intensity for ZnO samples supported on CP is an indication that there has been a reduction in the recombination of the photogenerated electron-hole pairs (Gupta *et al.* 2021). This effect is linked to the use of CP as a support, which presents in its spectrum of photoluminescence a robust and high intensity peak at 414 nm. This important role of support in reducing electron–hole recombination is reported in other studies (Mehrabadi & Faghihian 2019).

### 3.2. Photocatalytic evaluation

The effect of different factors, including the influence of radiation, efficiency of the support, amount of ZnO in the zeolite matrix, concentration of photocatalyst, initial pH of the solution and reuse of the material were evaluated for degradation of HCQ. The photocatalytic degradation of HCQ ($C_0 = 10$ mg $L^{-1}$) under UV-A radiation with 10%ZnOCP catalyst is shown in Figure 5(a) and with the 15%ZnOCP catalyst is shown in Figure 5(b). The results indicated that the best degradation profile was for the catalyst 15%ZnOCP at a concentration of 2 g $L^{-1}$, reaching 96% degradation. It is also possible to observe

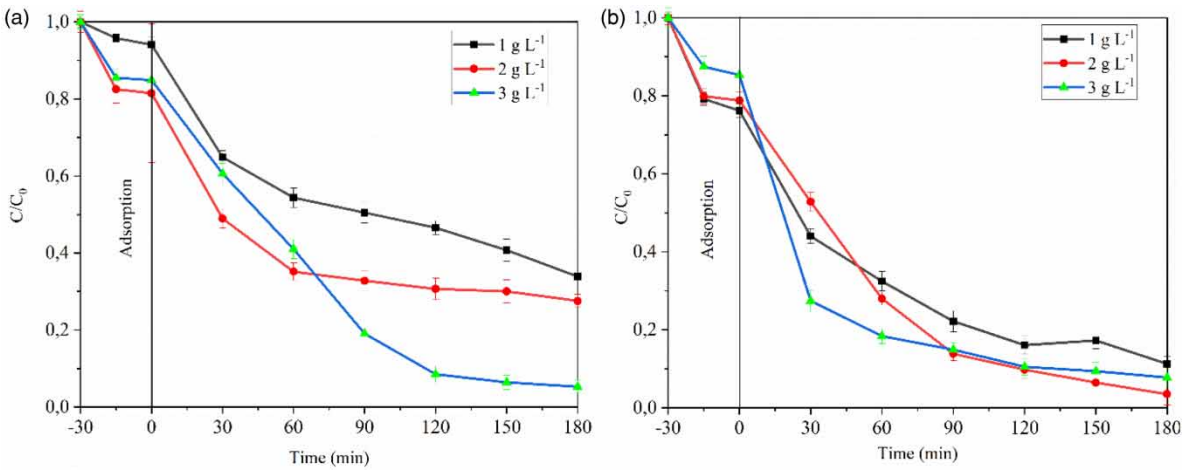


**Figure 5** | Degradation kinetics of HCQ ($C_0 = 10$ mg $L^{-1}$; pH = 7.5; radiation UV-A) (a) 10%ZnOCP (b) 15%ZnOCP.

that both catalysts showed good adsorption in the dark period, indicating that the compound formed by ZnOCP works as an effective adsorbent, due to existing electrostatic forces, as discussed in item 3.1.

The results of the analyzes carried out in triplicate were analyzed statically by means of the ANOVA test, performed by the software Statistica 10, using a significance level of 5% and a *p*-value less than 0.05 was obtained, therefore it was possible to state with 95% confidence that there are significant differences between the means of the variables. The statistical parameters of the ANOVA test can be found in Table S2 (Supporting Information). A more detailed discussion of each factor will be addressed in the following items.

### 3.2.1. ZnO loading effect

A very important parameter to be discussed is the effect of the ZnO load supported on the zeolite. This work studied two charges, 10 and 15% ZnO in zeolite. The results presented in Figure 5 show that the efficiency of the degradation increased as the ZnO loading increased in the zeolite matrix (Nezamzadeh-Ejhieh & Khodabakhshi-Chermahini 2014). This is because the increase in the ZnO charge causes an increase in the pairs of electron–hole and, therefore, an increase in the efficiency of degradation. The use of zeolite as a support for zinc oxide prevents aggregation of zinc oxide particles and, consequently, the photocatalytic process is improved. The increase in the rate of degradation can be explained by the increase in active sites available for the pollutant. (Heidari *et al.* 2020) obtained similar results when they studied the ZnO mass load in the zeolites for degradation of the drug furosemide. Their results confirmed that there is an increase in the rate of degradation due to the increase in the amount of ZnO, from 5 to 15%. However, an increase of more than 15% may cause an agglomeration of ZnO particles on the surface of the zeolite, which may reduce the photocatalytic capacity.

### 3.2.2. Catalysts weight effect

The effect of the catalyst dosage was studied in the range of 1–3 g $L^{-1}$. It is important that the catalyst dosage is adequate so that during the reaction a rate of generation of electron-hole pairs and formation of favorable OH radicals is obtained to increase the efficiency of photodegradation (Bahrami & Nezamzadeh-Ejhieh 2015).

For the catalyst supported with 10%ZnOCP, it appears that the increase in catalyst in the solution favors the photodegradation of the drug. This is expected, as an increase in catalyst provides a greater availability of active sites on the catalyst surface for adsorption and photoexcitation (Bansal & Sud 2011; Nezamzadeh-Ejhieh & Khodabakhshi-Chermahini 2014). The total area of the active surface increases with the increase of catalyst in the solution (Daneshvar *et al.* 2004), however, an excessive increase, in addition to the optimum value, causes some parts of the catalyst to remain in darkness due to the increase in turbidity of the solution and consequently, there is a decrease in the penetration of ultraviolet light, reducing the photocatalytic activity (Nezamzadeh-Ejhieh & Khodabakhshi-Chermahini 2014). This behavior is observed for the 15% ZnOCP catalyst, in which the best degradation efficiency is obtained using the dosage of 2 g $L^{-1}$, the increase in catalyst concentration resulted in a small reduction in the percentage of HCQ degradation to end of the reaction.

### 3.2.3. Radiation effect

To evaluate the effect of radiation on HCQ degradation, two radiation sources were used, UV-A lamps that emit longwave radiation in the range from 315 to 400 nm and natural solar radiation with an emission spectrum divided into high energy ultraviolet (5%), visible and infrared light with photothermal effect (Kim *et al.* 2019). Figure 6 shows the degradation profile of the compound under natural solar irradiation and UV-A ($C/C_0$) by the exposure time (min) without the presence of the catalyst (photolysis) and with the catalyst 15%ZnOCP at a concentration of 2 g $L^{-1}$. It can be seen that the use of natural solar radiation resulted in a higher percentage of HCQ degradation (48%), while UV-A radiation reached 25% degradation. According to Dabić *et al.* (2019), who conducted a study on the photodegradation of HCQ in environmental matrices through simulated sunlight, HCQ is susceptible to photodegradation in various environmental conditions and photolysis can occur and have a relevant impact on environmental fate.

In the presence of the catalyst, it is possible to evaluate that the degradation of HCQ was greater and faster with the use of natural sunlight. This result is quite interesting, since the use of natural sunlight reduces the costs of the process, in addition to being an environmentally friendly energy source with great availability in some regions. The higher efficiency and speed of HCQ solar photocatalysis can be attributed to the effect of solar photolysis, which contributes to a good percentage of degradation. Another factor to be considered is the characteristics of ZnO, which has a wide band gap (3.37 eV) and marked optical properties such as its high optical transparency in the visible range, which makes it an efficient degradation catalyst under sunlight (Sa-nguanprang *et al.* 2020).

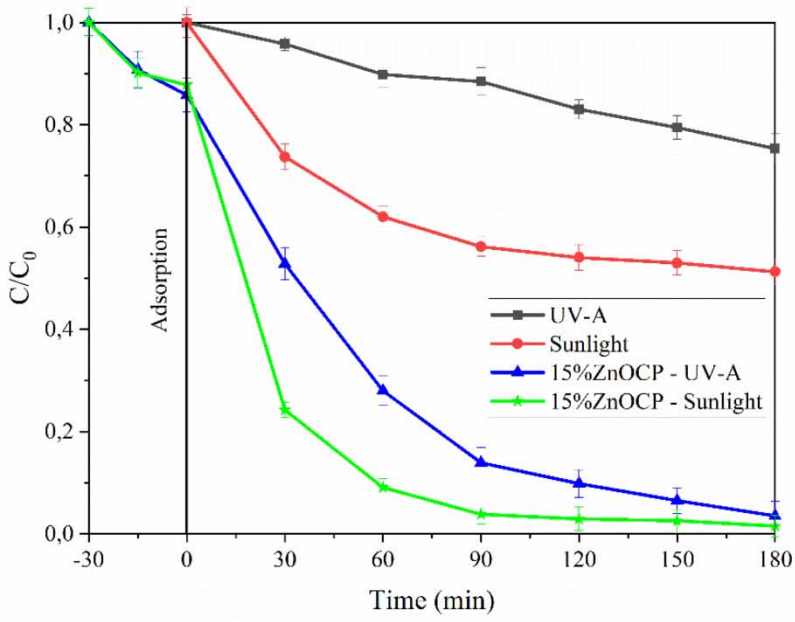


**Figure 6** | Effect of radiation on HCQ degradation.

### 3.2.4. Support effect

To evaluate the effect of the support, in the HCQ degradation process, commercial ZnO in suspension and ZnO catalysts supported in CP, at a concentration of 2 g $L^{-1}$ and UV-A radiation were used. Figure 7 shows the results of degradation ($C/C_0$) by the reaction time (min).

It is possible to evaluate that the percentage of degradation at the end of the 180 min of reaction was similar for the tested catalysts. However, analyzing the degradation profile of the catalysts, it is clear that the ZnO catalyst in

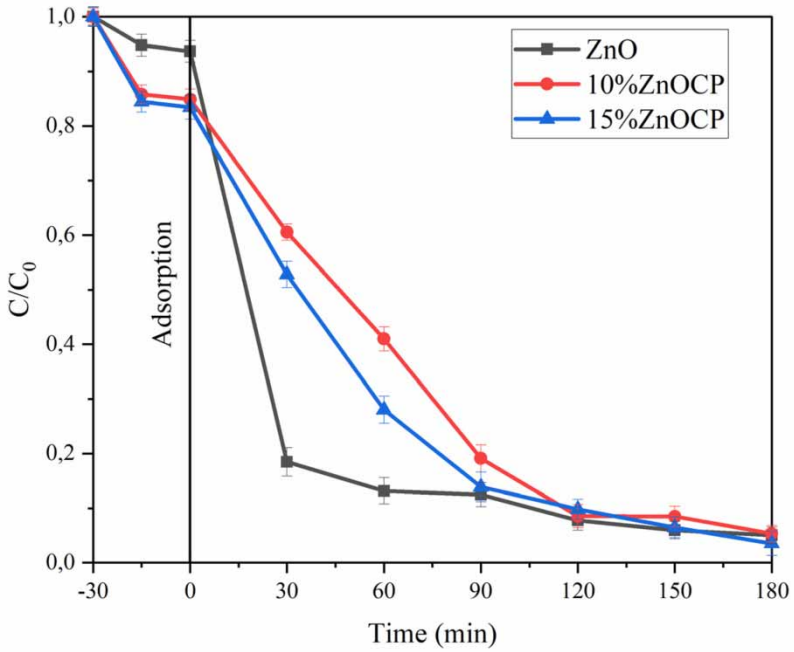


**Figure 7** | Effect of support on HCQ.

suspension showed a higher degradation speed than the supported catalysts, reaching around 80% removal in the first 30 min of photocatalytic reaction. This effect is not difficult to occur, since suspended catalysts have the advantage of a larger surface area for the reaction, more effective mass transport, a large illuminated surface area per unit volume of catalyst and minimal limitations on mass transfer (Diyanat *et al.* 2018). In addition, the introduction of ZnO particles in the zeolite pores makes it difficult to activate the catalyst by the radiation used, reducing the accessibility of the catalyst to photons and the number of active sites available and consequently reducing photocatalytic activity (Srikanth *et al.* 2017). However, as can be seen, catalysts supported on CP zeolite showed similar performance to ZnO in suspension, when the final percentage of HCQ degradation is evaluated. Thus, the CP zeolite can be considered a support with great potential for application in photocatalysis, with regard to photocatalytic activity, also standing out in the reduction of recombination of photogenerated electron-hole pairs, as discussed in Section 3.1.

### 3.2.5. Effect of initial pH

To investigate the effect of pH on the photocatalytic degradation of HCQ, tests were performed varying the initial pH of the solution (7.5) to a more acidic solution (4) and another more basic solution (10), using the most efficient catalyst, 15%ZnOCP, at a concentration of 2 g $L^{-1}$ irradiated by the UV-A lamp. The degradation kinetics of the tests are shown in Figure 8. It was verified that the removal efficiency happened without the variation of the initial pH of the solution. This result was positive, as it avoids the need to change the pH of the solution to maximize the degradation of the contaminant. Information about the influence of pH on HCQ photocatalysis is scarce in the literature. The effect of pH on the photocatalysis process is complex, as it involves parameters such as the semiconductor surface load, hydroxyl radical production and the nature of the substrate, which can interfere with the rate of degradation.

In this case, the presence of electrostatic forces present in the process helps to explain the greater degradation efficiency at natural pH, as discussed in Section 3.1. Other factors justify the reduction of the degradation efficiency at acidic pH, such as the agglomeration of the ZnO particles, decreasing the specific area for photons adsorption and absorption, in addition the fact that the solution is acidified using HCl, increases the amount of $Cl^-$ that could compete with the contaminant in the adsorption process or act as $HO^-$ hijackers (Fernández *et al.* 2004). At high pH, according to the literature, repulsion may occur between the catalyst surface and the contaminant molecule, by excluding charges, and between the catalyst surface and hydroxyl ions, decreasing the rate of formation of hydroxyl radicals (Habibi *et al.* 2005).

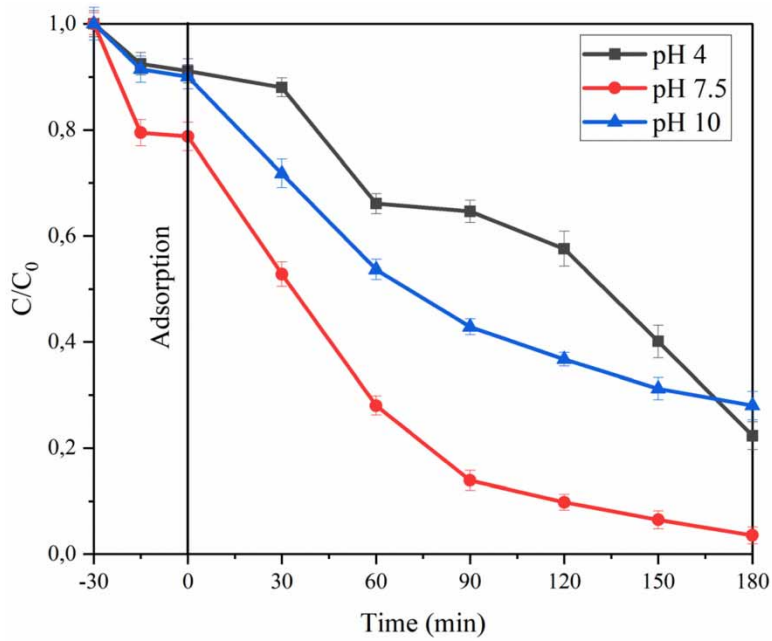


**Figure 8** | Effect of pH on HCQ degradation.

### 3.2.6. Reuse of catalysts

Catalyst reuse has been studied to obtain the best photodegradation conditions ($C_0 = 10$ mg $L^{-1}$; $C_{cat} = 2$ g $L^{-1}$ of 15% ZnOCP; pH = 7.5; radiation UV-A). After each use, the catalyst was filtered, washed and dried in an oven at 60 °C for 24 hours to remove impurities and subsequently subjected to a new use in order to verify its chemical stability. Based on the results presented in Figure S2 (Supplementary information), a decrease of about 8% was observed in relation to the first use and first reuse, which indicates that the catalyst did not significantly reduce its photoactivity. However, in the third reuse the decrease in the photocatalytic activity of the catalyst was 59%. Yener *et al.* (2017) states that the reduction in photocatalytic activity is due to the accumulation of contaminant on the surface of the catalyst, which leads to a reduction in adsorption due to the active sites being blocked by the pollutant molecules. For Bahrami & Nezamzadeh-Ejhieh (2015) this significant loss of catalyst efficiency can be attributed to the leaching of zinc cations in solution, which causes the photocatalytic activity of the semiconductor to decrease, together with the active sites on the surface of the catalyst. The results found in this article are in agreement with those of the authors Nezamzadeh-Ejhieh & Khodabakhshi-Chermahini (2014).

## 3.3. Toxicity tests

After conducting the photocatalytic tests, the effluent generated by the best conditions ($C_0 = 10$ mg $L^{-1}$; $C_{cat} = 2$ g $L^{-1}$ of 15% ZnOCP; pH = 7.5; radiation UV-A) was subjected to toxicity tests against the bioindicators *Lactuca sativa* and *Artemia salina*.

The tests with *Lactuca sativa* comprised triplicate series with negative control, positive control, samples of untreated synthetic effluent and samples of treated synthetic effluent. The results expressed in Table 2 show that 100% relative germination was achieved for the treated samples, while in the untreated it was 90%. The relative root growth for the treated sample was greater than 100%, that is, they grew more than the control roots, which indicated that the lettuce roots did not suffer growth inhibition by the treatment (RLR > 0.8) while that the untreated synthetic effluent sample demonstrated the occurrence of inhibitory effects (RLR < 0.8) (Aquino *et al.* 2019). It is possible that there was formation of nitrogenous nutrients during the degradation of HCQ, which acted as a source of growth for seeds.

The tests with *Artemia salina* are shown in Table 3 and were performed in quintuplicate for the control, untreated synthetic effluent and treated synthetic effluent. Through the results obtained after plotting the Reed–Muench graph, the average lethal concentration of the effluent without treatment was 158.48 mg $L^{-1}$. The treated effluent, on the other hand, had a lethal concentration greater than 200 mg $L^{-1}$, indicating that it was a non-toxic effluent after photodegradation.

From the results achieved, it can be said that both tests led to the conclusion that the 15%ZnOCP catalyst is effective for reducing toxicity in the oxidative treatment of HCQ.

**Table 2** | Toxicity assessment against *Lactuca sativa*

| | Germinated seed | Mean root length (cm) | Relative germination rate (%) | Relative length rate (%) |
|---|---|---|---|---|
| Negative control | 0 | 0 | 0 | 0 |
| Positive control | 10 | 2.54 ± 0.20 | 100 | 100 |
| Initial effluent | 9 | 1.84 ± 0.15 | 90 | 73 |
| Treated effluent | 10 | 2.75 ± 0.25 | 100 | 108 |

**Table 3** | Toxicity assessment against *Artemia salina*

| | $LC_{50}$ | Concentration (mg $L^{-1}$) | Mortality (%) |
|---|---|---|---|
| Control | 1.45 | 29.51 | 100 |
| Initial effluent | 1.72 | 158.48 | 97 |
| Treated effluent | 2.20 | >200.00 | 36 |

## 4. CONCLUSION

The characterization results obtained in this work showed that the synthesis to support ZnO in CP particles resulted in a good catalyst and advantageously low cost for HCQ photodegradation with UV-A radiation. The operational parameters were studied in order to evaluate their influence on the photodegradation process in the best experimental condition for an initial concentration of 10 mg $L^{-1}$ of HCQ was 2 g $L^{-1}$ of the catalyst 15%ZnOCP, pH = 7.5 and UV-A radiation. It was possible to observe that the photocatalytic activity decreased significantly after the first reuse, possibly due to the blocking of contaminant molecules on the catalyst surface. Ecotoxicological tests suggested that the toxicity of the synthetic effluent after the advanced oxidative treatment had been reduced.

## DATA AVAILABILITY STATEMENT

All relevant data are included in the paper or its Supplementary Information.

## REFERENCES


Aquino, R. V. S. d., Barbosa, A. A., Carvalho, R. F. d., Silva, M. G., Nascimento Júnior, W. J. d., Silva, T. D. d., Silva, J. P. & Rossiter Sá da Rocha, O. 2019 Degradation study of tris(2-butoxyethyl) phosphate with $TiO_2$ immobilized on aluminum meshes employing artificial neural networks. *Water Science and Technology: A Journal of the International Association on Water Pollution Research* **80** (6), 1163–1173.

Bahrami, M. & Nezamzadeh-Ejhieh, A. 2015 Effect of the supported ZnO on clinoptilolite nano-particles in the photodecolorization of semi-real sample bromothymol blue aqueous solution. *Materials Science in Semiconductor Processing* **30**, 275–284. http://dx.doi.org/10.1016/j.mssp.2014.10.006.

Bansal, P. & Sud, D. 2011 Photodegradation of commercial dye, Procion Blue HERD from real textile wastewater using nanocatalysts. *Desalination* **267** (2–3), 244–249. http://dx.doi.org/10.1016/j.desal.2010.09.034.

Batistela, V. R., Fogaça, L. Z., Fávaro, S. L., Caetano, W., Fernandes-Machado, N. R. C. & Hioka, N. 2017 ZnO supported on zeolites: photocatalyst design, microporosity and properties. *Colloids and Surfaces A: Physicochemical and Engineering Aspects* **513**, 20–27.

Borba, M. G. S., Val, F. F. A., Sampaio, V. S., Alexandre, M. A. A., Melo, G. C., Brito, M., Mourão, M. P. G., Brito-Sousa, J. D., Baía-da-Silva, D., Guerra, M. V. F., Hajjar, L. A., Pinto, R. C., Balieiro, A. A. S., Pacheco, A. G. F., Santos, J. D. O., Naveca, F. G., Xavier, M. S., Siqueira, A. M., Schwarzbold, A., Croda, J., Nogueira, M. L., Romero, G. A. S., Bassat, Q., Fontes, C. J., Albuquerque, B. C., Daniel-Ribeiro, C. T., Monteiro, W. M. & Lacerda, M. V. G. 2020 Effect of high vs low doses of chloroquine diphosphate as adjunctive therapy for patients hospitalized with severe acute respiratory syndrome coronavirus 2 (SARS-CoV-2) infection: a randomized clinical trial. *JAMA Network Open* **3** (4), e208857.

Browning, D. J. 2014 Pharmacology of chloroquine and hydroxychloroquine. In: *Hydroxychloroquine and Chloroquine Retinopathy*. Springer New York, New York, NY, pp. 35–63. Available from: http://link.springer.com/10.1007/978-1-4939-0597-3_2.

Chen, W. Y., Wu, Y. T., Lin, H. C., Ieong, M. I. & Lee, B. H. 2020 Impact of long-term parental exposure to Tamiflu metabolites on the development medaka offspring (*Oryzias latipes*). *Environmental Pollution* **261**, 114–146. https://doi.org/10.1016/j.envpol.2020.114146.

Dabić, D., Babić, S. & Škorić, I. 2019 The role of photodegradation in the environmental fate of hydroxychloroquine. *Chemosphere* **230**, 268–277.

Daneshvar, N., Salari, D. & Khataee, A. R. 2004 Photocatalytic degradation of azo dye acid red 14 in water on ZnO as an alternative catalyst to $TiO_2$. *Journal of Photochemistry and Photobiology A: Chemistry* **162** (2–3), 317–322.

Daughton, C. G. 2014 The matthew effect and widely prescribed pharmaceuticals lacking environmental monitoring: case study of an exposure-assessment vulnerability. *Science of the Total Environment* **466–467**, 315–325. http://dx.doi.org/10.1016/j.scitotenv.2013.06.111.

Diyanat, S., Homaei, A. & Mosaddegh, E. 2018 Immobilization of *Penaeus vannamei* protease on ZnO nanoparticles for long-term use. *International Journal of Biological Macromolecules* **118**, 92–98. https://doi.org/10.1016/j.ijbiomac.2018.06.075.

Dobrucka, R. & Długaszewska, J. 2016 Biosynthesis and antibacterial activity of ZnO nanoparticles using *Trifolium pratense* flower extract. *Saudi Journal of Biological Sciences* **23** (4), 517–523.

Fernández, J., Kiwi, J., Baeza, J., Freer, J., Lizama, C. & Mansilla, H. D. 2004 Orange II photocatalysis on immobilised $TiO_2$: effect of the pH and $H_2O_2$. *Applied Catalysis B: Environmental* **48** (3), 205–211.

Gupta, J., Hassan, P. A. & Barick, K. C. 2021 Structural, photoluminescence, and photocatalytic properties of Mn and Eu co-doped ZnO nanoparticles. *Materials Today: Proceedings* **42** (2), 926–931. https://doi.org/10.1016/j.matpr.2020.11.837.

Gutul, T., Rusu, E., Condur, N., Ursaki, V., Goncearenco, E. & Vlazan, P. 2014 Preparation of poly(*N*-vinylpyrrolidone)-stabilized ZnO colloid nanoparticles. *Beilstein Journal of Nanotechnology* **5** (1), 402–406.

Habibi, M. H., Hassanzadeh, A. & Mahdavi, S. 2005 The effect of operational parameters on the photocatalytic degradation of three textile azo dyes in aqueous $TiO_2$ suspensions. *Journal of Photochemistry and Photobiology A: Chemistry* **172** (1), 89–96.

Heidari, Z., Alizadeh, R., Ebadi, A., Oturan, N. & Oturan, M. A. 2020 Efficient photocatalytic degradation of furosemide by a novel sonoprecipited ZnO over ion exchanged clinoptilolite nanorods. *Separation and Purification Technology* **242** (January), 116800. https://doi.org/10.1016/j.seppur.2020.116800.

Kim, J. H., Lee, H. K., Park, Y. J., Lee, S. B., Choi, S. J., Oh, W., Kim, H. S., Kim, C. R., Kim, K. C. & Seo, B. C. 2019 Studies on decomposition behavior of oxalic acid waste by UVC photo-Fenton advanced oxidation process. *Nuclear Engineering and Technology* **51** (8), 1957–1963. https://doi.org/10.1016/j.net.2019.06.011.

Mehrabadi, Z. & Faghihian, H. 2019 Clinoptilolite modified with $TiO_2$ for simultaneous elimination of two herbicides; 2,4-D and MCPA by UV and sunlight-assisted photocatalytic degradation. *Materials Research Bulletin* **119** (December 2018), 110569. https://doi.org/10.1016/j.materresbull.2019.110569.

Meyer, B. N., Ferrigni, N. R., Putnam, J. E., Jacobsen, L. B., Nichols, D. E. & McLaughlin, J. L. 1982 Brine shrimp: a convenient general bioassay for active plant constituents. *Planta Medica* **45** (1), 31–34.

Nezamzadeh-Ejhieh, A. & Khodabakhshi-Chermahini, F. 2014 Incorporated ZnO onto nano clinoptilolite particles as the active centers in the photodegradation of phenylhydrazine. *Journal of Industrial and Engineering Chemistry* **20** (2), 695–704. http://dx.doi.org/10.1016/j.jiec.2013.05.035.

Piedra López, J. G., González Pichardo, O. H., Pinedo Escobar, J. A., de Haro del Río, D. A., Inchaurregui Méndez, H. & González Rodríguez, L. M. 2021 Photocatalytic degradation of metoprolol in aqueous medium using a $TiO_2$/natural zeolite composite. *Fuel* **284** (August 2020), 119030. https://doi.org/10.1016/j.fuel.2020.119030.

Rathore, A. K., Pati, S. P., Ghosh, M., Roychowdhury, A. & Das, D. 2017 Effect of ZnO coating on two different sized $\alpha$-Fe nanoparticles: synthesis and detailed investigation of their structural, optical, hyperfine and magnetic characteristics. *Journal of Materials Science: Materials in Electronics* **28** (9), 6950–6958.

Roychowdhury, A., Pati, S. P., Mishra, A. K., Kumar, S. & Das, D. 2013 Magnetically addressable fluorescent $Fe_3O_4$/ZnO nanocomposites: structural, optical and magnetization studies. *Journal of Physics and Chemistry of Solids* **74** (6), 811–818. http://dx.doi.org/10.1016/j.jpcs.2013.01.012.

Sacco, O., Vaiano, V. & Matarangolo, M. 2018 ZnO supported on zeolite pellets as efficient catalytic system for the removal of caffeine by adsorption and photocatalysis. *Separation and Purification Technology* **193** (October 2017), 303–310.

Sa-nguanprang, S., Phuruangrat, A., Thongtem, T. & Thongtem, S. 2020 Characterization and photocatalysis of visible-light-driven Dy-doped ZnO nanoparticles synthesized by tartaric acid-assisted combustion method. *Inorganic Chemistry Communications* **117** (April), 107944. https://doi.org/10.1016/j.inoche.2020.107944.

Shen, Y., Zhou, P., Zhao, S., Li, A., Chen, Y., Bai, J., Han, C., Wei, D. & Ao, Y. 2020 Synthesis of high-efficient $TiO_2$/clinoptilolite photocatalyst for complete degradation of xanthate. *Minerals Engineering* **159** (July), 106640. https://doi.org/10.1016/j.mineng.2020.106640.

Srikanth, B., Goutham, R., Badri Narayan, R., Ramprasath, A., Gopinath, K. P. & Sankaranarayanan, A. R. 2017 Recent advancements in supporting materials for immobilised photocatalytic applications in waste water treatment. *Journal of Environmental Management* **200**, 60–78. http://dx.doi.org/10.1016/j.jenvman.2017.05.063.

Tan, Y., Li, C., Sun, Z., Liang, C. & Zheng, S. 2020 Ternary structural assembly of BiOCl/$TiO_2$/clinoptilolite composite: study of coupled mechanism and photocatalytic performance. *Journal of Colloid and Interface Science* **564**, 143–154. https://doi.org/10.1016/j.jcis.2019.12.116.

Trujillo, M. E., Hirales, D., Rincón, M. E., Hinojosa, J. F., Leyva, G. L. & Castillón, F. F. 2013 $TiO_2$/clinoptilolite composites for photocatalytic degradation of anionic and cationic contaminants. *Journal of Materials Science* **48** (19), 6778–6785.

USEPA 1996 Ecological effects test guidelines OPPTS (850.4200): seed germination/root elongation toxicity test. *United States Environmental Protection Agency* (April), **1**, 1–8.

Yener, H. B., Yılmaz, M., Deliismail, Ö., Özkan, S. F. & Helvacı, Ş. Ş. 2017 Clinoptilolite supported rutile $TiO_2$ composites: synthesis, characterization, and photocatalytic activity on the degradation of terephthalic acid. *Separation and Purification Technology* **173**, 17–26. http://dx.doi.org/10.1016/j.seppur.2016.09.010.

Zhao, L. & Yu, J. 2006 Controlled synthesis of highly dispersed $TiO_2$ nanoparticles using SBA-15 as hard template. *Journal of Colloid and Interface Science* **304** (1), 84–91.

First received 30 April 2021; accepted in revised form 24 June 2021. Available online 6 July 2021